Sensors and Materials, Vol. 19, No. 3 (2007) 133–147
MYU Tokyo

S & M 0671

Frequency-Dependent Rectification of the Bidirectionally Oscillating Dynamic Flow in Microdiffusers

Young-Ho Lee and Young-Ho Cho*

Digital Nanolocomotion Center, Department of BioSystems,
Korea Advanced Institute of Science and Technology,
373-1 Gusong-dong, Yuseong-gu, Daejeon 305-701, Republic of Korea

(Received September 20, 2006; accepted March 27, 2007)

Key words: microdiffuser, bi-directional flow, oscillating flow, flow rectification, valveless pump

We characterize a bidirectionally oscillating dynamic flow in planar microdiffusers to investigate the frequency dependence of the flow rates and flow rectification performance of the microdiffuser. In the theoretical study, we present a bidirectionally oscillating flow model, where the boundary layer thickness governs the flow rectification performance of the microdiffusers. In the experimental study, we fabricate two types of microdiffusers, D100 and D300, having different neck widths of 100 μm and 300 μm, respectively. The net flow rates of the microdiffusers are measured for various pumping pressures and frequencies. The microdiffusers, D100 and D300, show maximum net flow rates of 116.6 μl/min and 344.4 μl/min, respectively, for an identical sinusoidal pumping pressure input of 1.6 kPa at 50 Hz. When the boundary layer thickness is greater than the neck width, the flow rates measured for D100 and D300 are approximately 47% of the theoretical values estimated using the conventional unidirectional static flow model. The experimental flow rate of D300, however, decreases at the rate of 0.18 %/Hz in the pumping frequency region higher than 90 Hz, when the boundary layer thickness is reduced to the microdiffuser neck width. Consequently, the frequency dependence of the net flow rates and the rectification performance of the planar microdiffusers are quantitatively evaluated in terms of the neck width and the boundary layer thickness developed in the bidirectionally oscillating microdiffuser flow.

1. Introduction

Recently, flow-rectifying microdevices[1–11] have received increasing attention for applications to precision micropumps, pressure regulators and flow controllers in

*Corresponding author: e-mail: nanosys@kaist.ac.kr

biochemical microsystems,[12,13] and have included microcheck valves[1–5] and valveless microdiffusers.[6–11] Among them, microdiffusers[6–11] have received more interest than microcheck valves,[1–5] due to their advantages of simple structure, high reliability, long lifetime and low cost. Microdiffusers also show strong potential for valveless microfluidic devices and system applications.

In the previous microdiffuser research,[6–11] the flow rectification performance of the microdiffusers was characterized on the basis of a unidirectional static flow model, where the net flow rate was estimated from the superposition of two uni-directional flows. In this paper, however, we present a bidirectionally oscillating dynamic flow model for the microdiffuser analysis, thereby evaluating the net flow rates and the frequency dependence of the rectification performance of the microdiffusers. We fabricated a set of microdiffuser prototypes, from which the frequency dependence of the flow rates and flow rectification performance were measured and discussed. We quantitatively evaluated the bidirectionally oscillating dynamic flow in the microdiffusers by comparing the experimental results with the theoretical values.

2. Microflow Models and Theoretical Analysis

Figure 1 shows the flow rectifying function of microdiffusers. In this paper, we consider a microdiffuser system (Fig. 2(a)), composed of three chambers connected by two identical microdiffusers shown in Fig. 2(b). The three chambers in Fig. 2(a) correspond to the inlet chamber, the pump chamber and the outlet chamber shown in Fig. 1.

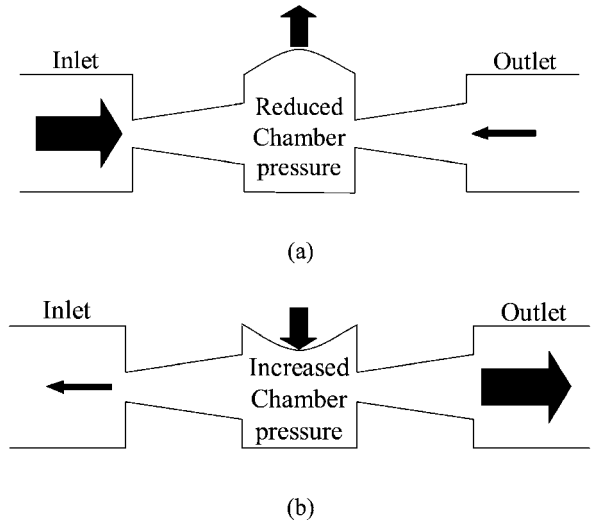

Fig. 1. Flow-rectifying microdiffusers: (a) intake cycle reduces chamber pressure by increasing the chamber volume, (b) outtake cycle increases chamber pressure by decreasing the chamber volume.

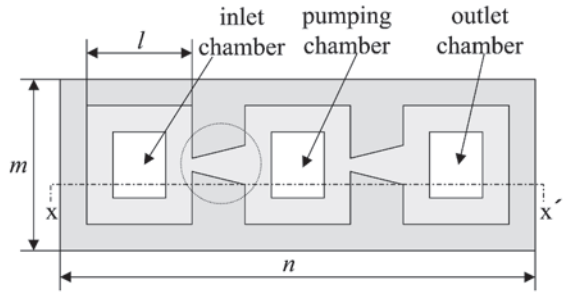

(a)

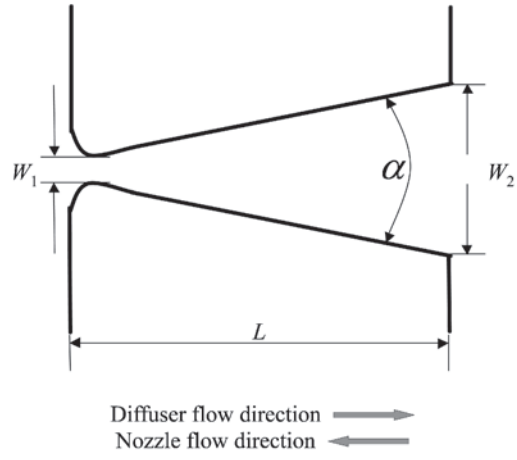

(b)

Fig. 2. Three chambers connected by microdiffusers: (a) top view, (b) enlarged view of the microdiffuser, whose dimensions are listed in Table 1.

2.1 *Unidirectional static flow*

In the unidirectional static flow model,[6–11] the microflow in the microdiffusers is considered as the combination of two unidirectional flows: the diffusion flow and the nozzle flow indicated in Fig. 2(b). For each flow direction, the pressure loss coefficient, ξ, of the microdiffuser (Fig. 2(b)) is defined[7] as the ratio of the pressure drop to the flow kinetic energy:

$$\xi = 2\,\frac{\Delta P}{\rho \bar{u}^2}, \tag{1}$$

where $\bar{u}$ is the mean flow velocity in the microdiffuser neck, ρ is the fluid density and ΔP is the pressure drop across the microdiffuser.

For the flow rectification function of the microdiffusers, the pressure loss coefficient in the diffuser flow direction has to be lower than that in the nozzle flow direction. This condition can be stated[8] by the diffuser efficiency ratio, η, being greater than 1.

$$\eta = \frac{\xi_{nozzle}}{\xi_{diff}} \rangle\ 1, \tag{2}$$

where ξ_{nozzle} and ξ_{diff} are the pressure loss coefficient in the diffuser flow direction and that in the nozzle flow direction, respectively.

From eq. (1), the net flow rate of the microdiffuser is expressed as

$$Q_{estimated} = (\beta_1 - \beta_2)\sqrt{\Delta P} \tag{3}$$

In eq. (3), the term($\beta_1 - \beta_2$) is considered as the valve efficiency or the flow rectification efficiency of the microdiffuser, where β_1 is the coefficient in the diffuser flow direction and β_2 is the coefficient in the nozzle flow direction:

$$\beta_1 = A_1\sqrt{\frac{2}{\rho\xi_{diff}}} \tag{4}$$

$$\beta_2 = A_1\sqrt{\frac{2}{\rho\xi_{nozzle}}} \tag{5}$$

2.2 *Bidirectional oscillating flow*

For the oscillatory pumping of the fluid through the microdiffuser, however, the pressure and flow directions in the microdiffuser are rapidly changing. In this case, we consider that the key parameter affecting the flow rectification performance of the microdiffuser is the thickness of the boundary layer developed by the bidirectionally oscillating flow in the microdiffuser. Thus, the net flow rate and the flow rectification efficiency estimated using the previously mentioned unidirectional flow model would be valid only for a fully developed microdiffuser flow at a low oscillating frequency. This is because unidirectional flow model is based on the assumption of a fully developed boundary layer, the boundary layer cannot become fully developed before the flow direction changes in the microdiffuser; thus the thickness of the boundary layer might be a function of the oscillating frequency. For the case of high-frequency fluid pumping, the effect of the bidirectional oscillating flow should be considered for more realistic microdiffuser analysis.

For the bidirectionally oscillating flow, the boundary layer thickness of the microdiffuser flow can be estimated using the Stokes' second problem[14] shown in Fig. 3(a):

$$\frac{\partial u}{\partial t} = \nu\ \frac{\partial^2 u}{\partial y^2}, \tag{6}$$

where ν is the kinematic viscosity of the fluid and y is the normal distance from the microdiffuser wall. For the oscillating frequency, ω, the velocity profile along the diffuser wall is given[14] as

(a)

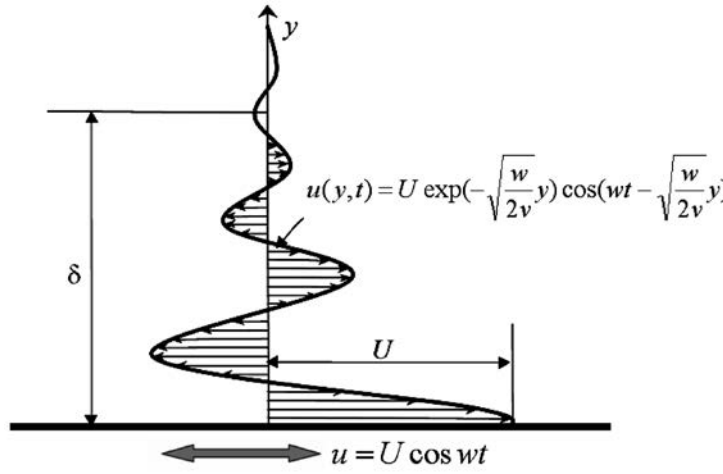

(b)

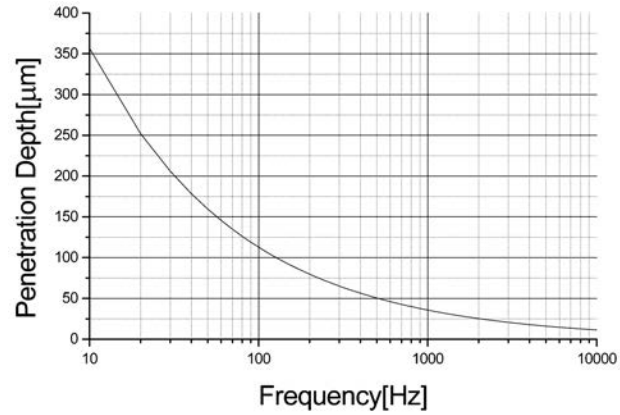

Fig. 3. Boundary layer developed in the oscillating flow: (a) velocity profile of Stokes' second problem, (b) boundary layer thickness for various oscillating flow frequencies.

$$\frac{u(y,t)}{U} = \exp(-\sqrt{\frac{\omega}{2v}}\, y)\cos(\omega t - \sqrt{\frac{\omega}{2v}}\, y), \tag{7}$$

The boundary layer thickness, δ, of the bidirectionally oscillating flow is defined by the distance between the wall and the point where the amplitude of flow motion, u, is $1/e^2$ of its maximum value, U. From eq. (7), we obtain the boundary layer thickness, δ, as

$$\delta = 2\sqrt{\frac{2v}{\omega}}, \tag{8}$$

For water (v=1.12×10^{-6} m^2/s at 15.6°C), the frequency dependence of the boundary layer thickness is estimated, as shown in Fig. 3(b). For the flow frequency of 100 Hz,

the boundary layer thickness developed in the microdiffuser is obtained as 113 μm. We consider that the fluid at the location far away from the boundary layer thickness, δ, is essentially unaffected by the fluid viscosity.

3. Design and Microfabrication of Microdiffusers

In the present study, we focus on the effect of the diffuser neck width, W_1, on the net flow rate and the flow rectification performance of microdiffusers. From eq. (8), we obtain the boundary layer thicknesses, δ, of 50 μm and 150 μm for the microdiffuser flow oscillating at the frequency of 500 Hz and 57 Hz, respectively. We design two microdiffusers, D100 and D300, having neck widths of 100 μm and 300 μm, respectively. In other words, the neck widths of the microdiffuser prototypes, D100 and D300, are determined by the total boundary layer thicknesses developed at the flow frequencies of 500 Hz and 57 Hz, respectively. The divergence angle, α, and the dimensionless length, L/W_1, of the microdiffusers are maintained[9] as 7° and 13.7, respectively. Thus, the length, L, of the microdiffuser, D100, is 1.37 mm and that of the D300 is 4.11 mm. The depth, b, of both microdiffusers is 40 μm. Considering the zero divergence angle formed by the top and bottom surfaces of the microdiffusers, we assume the velocity profile of a fully developed flow along the direction normal to the microdiffusers. Table 1 summarizes the dimensions of the designed microdiffusers, whose dimensions in Fig. 2(a) are l=8 mm, m=16 mm and n=40 mm.

The microfabrication process for the microdiffusers is shown in Fig. 4. The fabrication process starts with the thermal growth (Fig. 4(a)) of 1.5 μm-thick silicon dioxide layers on the 4" 520 μm-thick (100) silicon wafers. In Fig. 4(b), the silicon dioxide layers are patterned by Reactive Ion Enhanced etching (RIE) using a PR mask. After the PR removal, the deep RIE defines the 40 μm-deep microdiffusers and chambers of Fig. 2(a) using the oxide mask as shown in Fig. 4(b). In Fig. 4(c), the removal of the thermal silicon dioxide using BOE solution is followed by the LPCVD of a 2000 Å-thick silicon nitride layer. After the silicon nitride layer is patterned by RIE on the backside of the wafer (Fig. 4(d)), the silicon wafer is etched in KOH solution (Fig. 4(e)). Finally, the silicon nitride layer is removed by boiling in H_3PO_4 (Fig. 4(f)). Figure 5 shows a top view SEM image of the fabricated microdiffuser.

Table 1
Dimensions of the microdiffuser prototypes of Fig. 2(b).

Microdiffuser prototype	Neck width, W_1	Width-length ratio, L/W_1	Length, L	Depth, b	Divergence angle, α
D100	100 μm	13.7	1,370 μm	40 μm	7°
D300	300 μm	13.7	4,110 μm	40 μm	7°

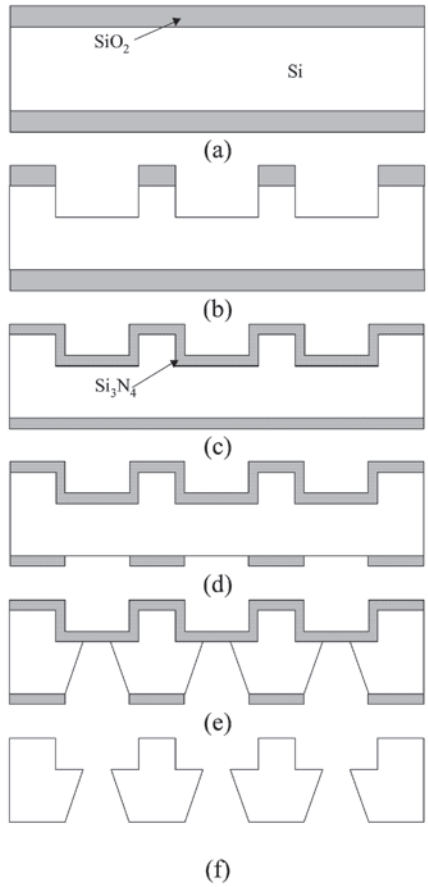

Fig. 4. Fabrication process for the microdiffusers: the cross-sectional view of Fig. 2(a) along the line, x-x'.

4. Experimental Apparatus and Measurements

Figure 6 shows the experimental apparatus for the microdiffuser test. As shown in Fig. 6(a), two feed holes and a rectangular hole for the diaphragm are fabricated by laser micromachining on a 500 μm-thick Pyrex glass plate before the glass is anodically bonded to the fabricated microdiffuser and the pumping chamber shown in Fig. 2(a) is covered by 100 μm-thick polymer film using epoxy adhesive. The lower part of the device shown in Fig. 6(a) is placed on a 2 mm-thick aluminum jig and 1 mm-thick silicone rubber. The silicone rubber is placed on a pressure sensor array (Autonics, PSA-01), whose sensing range is 0.1–5,000 Pa. We attached a multilayer piezoelectric actuator on the top of the polymer film shown in Fig. 6(a). The multilayer piezoelectric

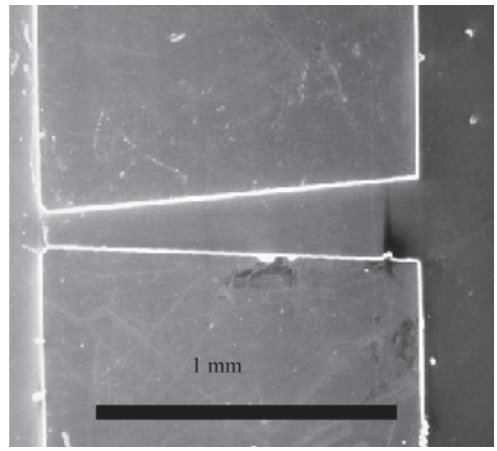

Fig. 5. SEM image of the fabricated microdiffuser shown in Fig. 2(b).

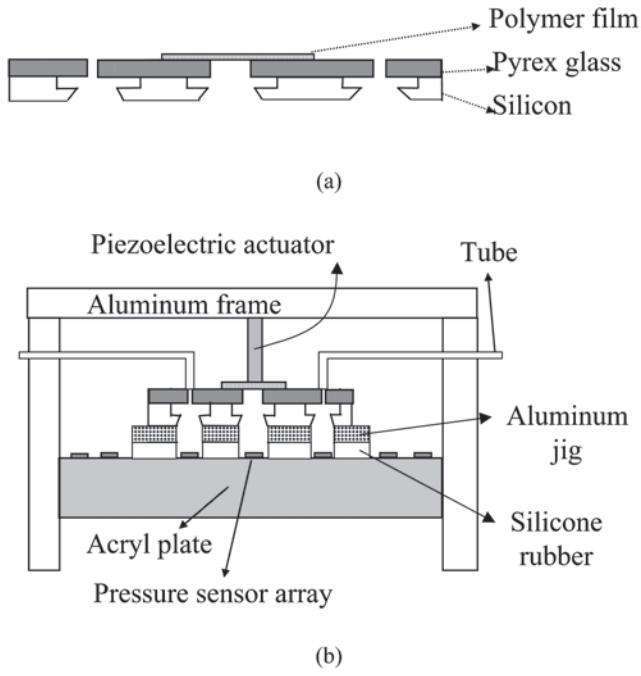

Fig. 6. Experimental apparatus: (a) microdiffuser assembly, (b) assembly of the experimental apparatus.

actuator is 2×3×18 mm^3, and its displacement response is 6 μm by a supplied 100 $V_{p\text{-}p}$ electrical signal. We assemble the experimental apparatus shown in Fig. 6(b) using an aluminum frame, which fixed the entire set of the pressure sensor array, the silicone rubber layer, the aluminum jig, the part shown in Fig. 6(a) and the piezoelectric actuator.

The inlet and outlet chambers are connected using a flexible Tygon® tubes, having an inner diameter of 1.59 mm. Figure 7(a) shows a photograph of the assembled test apparatus. We fill the test apparatus with deionized (DI) water through the tubes. To remove the air bubbles in the chambers and the microdiffusers, we pass CO_2 gas through the assembled apparatus for 20 min before filling with water. Because of the high solubility of CO_2 gas in water, we succeeded to prime the water into the experimental apparatus without residual bubbles.

Figure 7(b) shows the instrument setup using the assembled experimental apparatus shown in Fig. 7(a). We generate the pumping actuation at the pump chamber shown in Fig. 2(a) by supplying an AC signal to the piezoelectric actuator, while measuring the net flow rate from the distance traveled by the water in the tube. The dynamic pressures in the inlet, pump, and outlet chambers were measured using the pressure sensor

(a)

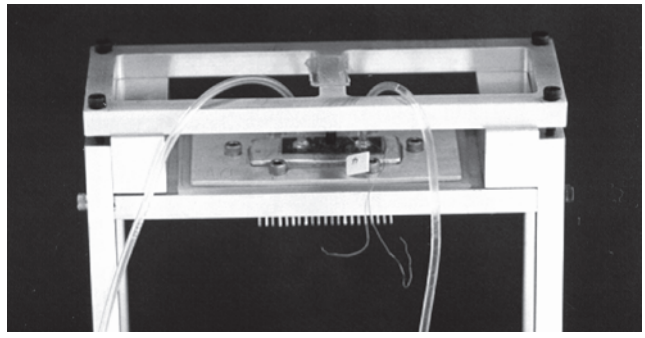

(b)

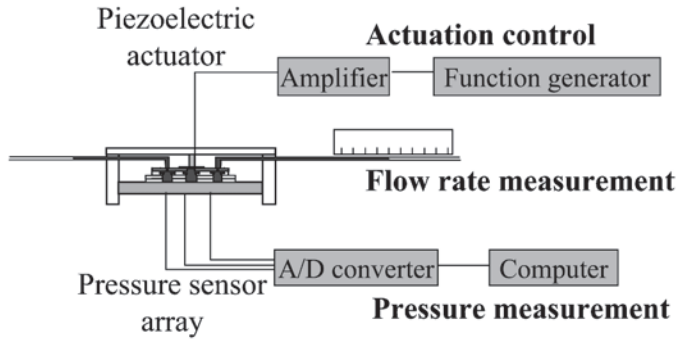

Fig. 7. Instrumentation setup for microdiffuser test: (a) photograph of the experimental apparatus, (b) measurements and instrumentation.

array. Thus, we measure the net flow rate passing through the microdiffusers as well as the pressures of the three chambers while varying the pumping frequency at the four sinusoidal voltages of 20, 40, 60 and 100 $V_{p\text{-}p}$ supplied to the piezoelectric actuator.

5. Experimental Results and Discussion

Figure 8 shows the frequency dependence of the net flow rates measured in the D100 and D300 microdiffusers. D100 and D300 show maximum net flow rates of 117 μl/min and 344 μl/min, respectively, for an identical piezoelectric actuation generated by the sinusoidal drive voltage of 100 $V_{p\text{-}p}$ at 50 Hz.

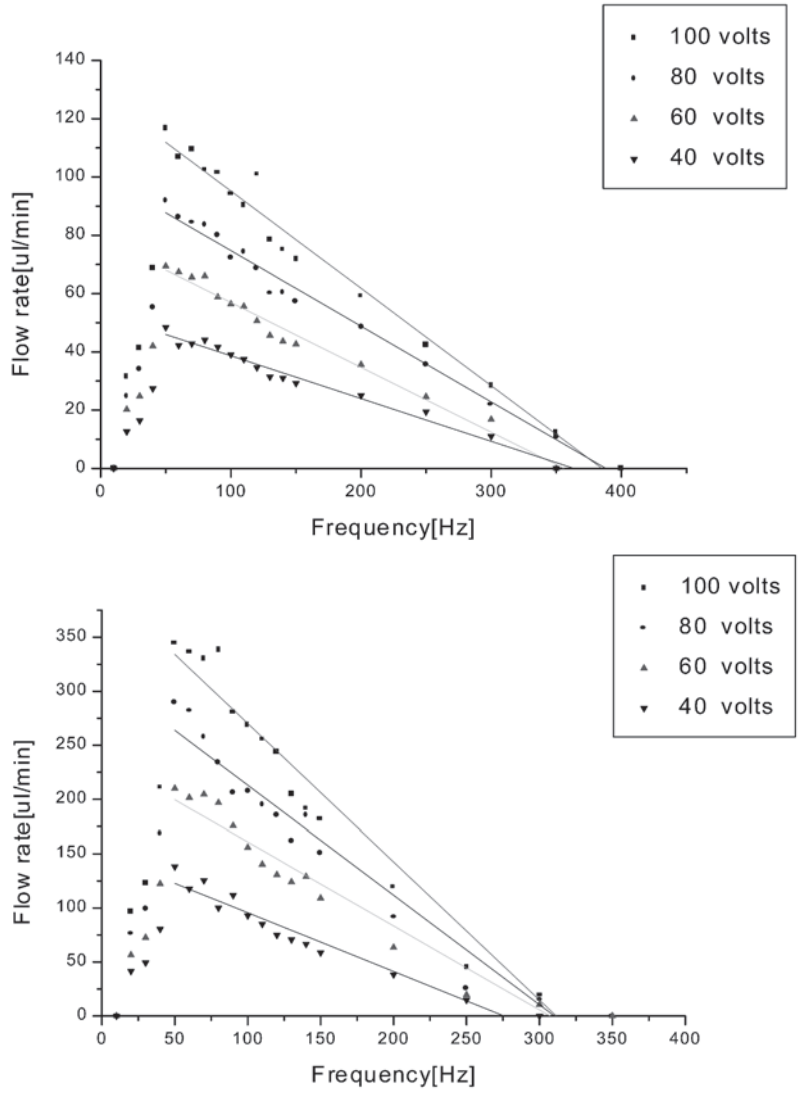

Fig. 8. Measured unidirectional net flow rates for various pump frequencies: (a) microdiffuser prototype D100, (b) microdiffuser prototype D300.

The pressures measured in the inlet and outlet of chambers shown in Fig. 2(a) is almost identical to atmospheric pressure; thus, the pressure in the pump chamber is considered as the pressure difference across the microdiffuser shown in Fig. 2(b). Figure 9 shows the frequency dependence of the pressure drops measured in D100 and D300. Each point in Fig. 9 shows the peak value of the sinusoidal behavior of the measured pressure at each frequency generated by the sinusoidal drive of the piezoelectric actuator. The maximum pressure drops of D100 and D300 are measured as 1.618 kPa and 1.595 kPa, respectively, resulting in an approximately equal value of 1.6 kPa for the piezoelectric actuation obtained from the sinusoidal drive voltage of 100 $V_{p\text{-}p}$ at 50 Hz.

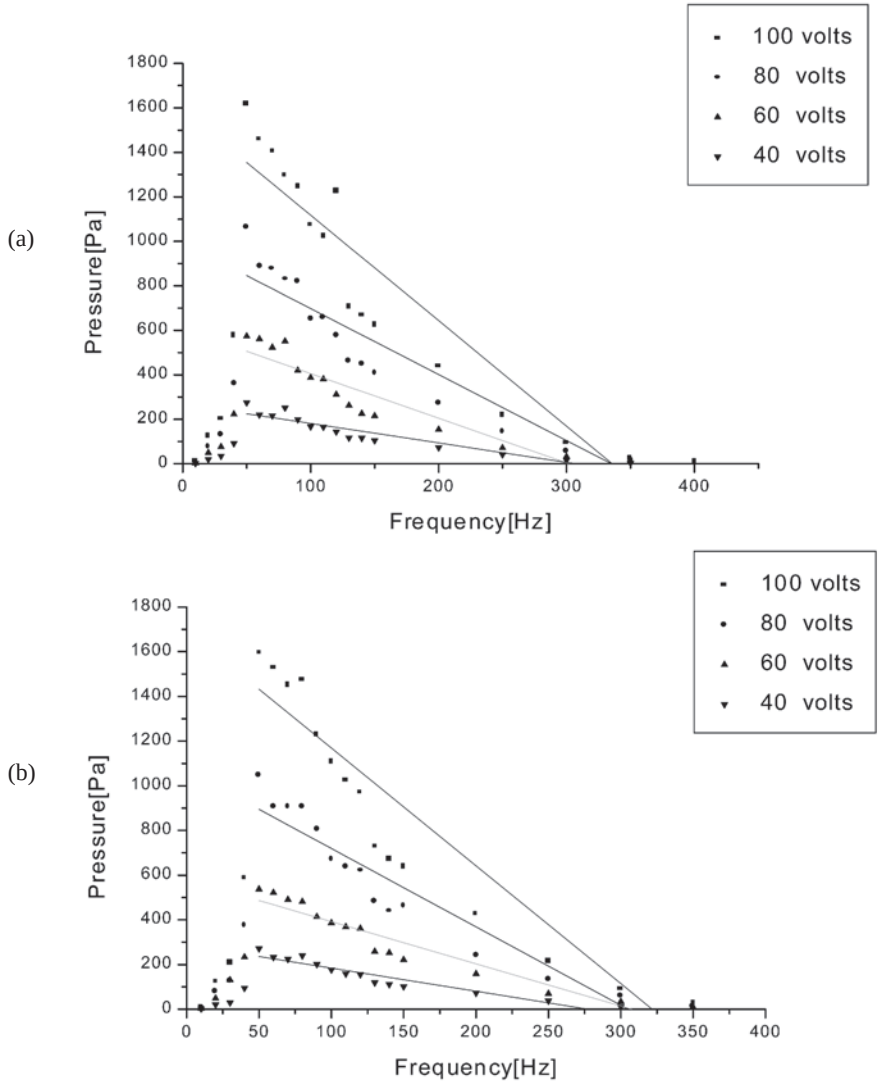

Fig. 9. Measured pump chamber pressure for various pump frequencies: (a) microdiffuser prototype D100, (b) microdiffuser prototype D300.

We estimate the flow rates of the microdiffusers from eq. (3) of unidirectional flow model by using the estimated value of β_1 and β_2 from eqs. (4) and (5), respectively, and the measured value of ΔP from Fig. 9. For the estimation of β_1 and β_2, we used the values of ξ_{diff} and ξ_{nozzle} as 0.33 and 1.07,[8] respectively. The maximum flow rates of D100 and D300 are estimated as 247 μl/min and 733 μl/min, respectively, on the basis of the pressure distribution in Fig. 9, which is supplied by the sinusoidal piezoelectric actuation voltage of 100 $V_{p\text{-}p}$ at 50 Hz to the assembled micropump structure. Using Fig. 8, we obtain the ratio of the measured flow rate to the estimated ratio, thus obtaining Fig. 10. In the Fig. 10, the uncertainty becomes larger toward both end frequencies, because the measured values become smaller, whereas the measurement error remains constant. this could explain the relatively low value at about 350 Hz shown in Fig. 10(a)

Figure 10(a) shows that for D100, the experimental flow rates are smaller than the theoretical values estimated from the static diffuser flow, with a constant reduction ratio of 46.5±6.2% in the frequency range of 20–350 Hz. The frequency independent valve efficiency, $(\beta_1–\beta_2)$ of eq. (3), is estimated as 1.34×10^{-10} from the unidirectional flow model, whereas the frequency dependent valve efficiency is estimated as 6.33×10^{-11} at 50 Hz and 6.27×10^{-11} at 250 Hz from the experimental results shown in Fig. 9.

The discrepancy between the measured net flow rate and the estimated flow rate can be explained by two reasons. First, the estimated flow rate is based on unidirectional turbulent flow.[8] In our experiment, however, the flow in the microdiffuser is bidirectional laminar flow. Generally, the Reynolds number is expressed by

$$\mathrm{Re} = \frac{\rho \bar{u} D}{\mu}, \tag{9}$$

where, ρ is the density, $\bar{u}$ is average velocity, D is the characteristic length, and μ is the dynamic viscosity. In this case, the Reynolds number can be modified as follows:

$$\mathrm{Re} = \frac{\rho \bar{u} D}{\mu} = \frac{\bar{u} w}{v} = \frac{\bar{u} w d}{v d} = \frac{\bar{u} A}{v d} = \frac{Q}{v d}, \tag{10}$$

where w, d and A are the width, depth (d=40 μm), and area of the nozzle/diffuser, respectively, Q is the volume flow rate and v is the kinematic viscosity (v=1.12×10^{-6} m²/s at 15.6°C). Thus, the maximum Reynolds number is at Q=246.7 μl/min (the maximum value of D100), and the value is about 90. For the case of D300, the Reynolds number is estimated as about 270.

The other reason is that, when we estimate the flow rate, we used the peak value of the sinusoidal behavior of the measured pressure at each frequency. This may cause the overestimation of the estimated flow rate values.

Figure 10(b) shows that the flow rate measured in D300 results in a constant reduction ratio of 46.5±6.2% in the flow frequency range of 20–80 Hz. The normalized experimental net flow rate, however, starts to decrease at frequencies greater than 90 Hz. The cutoff frequency of 90 Hz in Fig. 10(b) supports the validity of the oscillating flow model, where that the boundary layer thickness decreases to the microdiffuser neck width at the bidirectional flow frequency of 57 Hz. The discrepancy between the measured

(a)

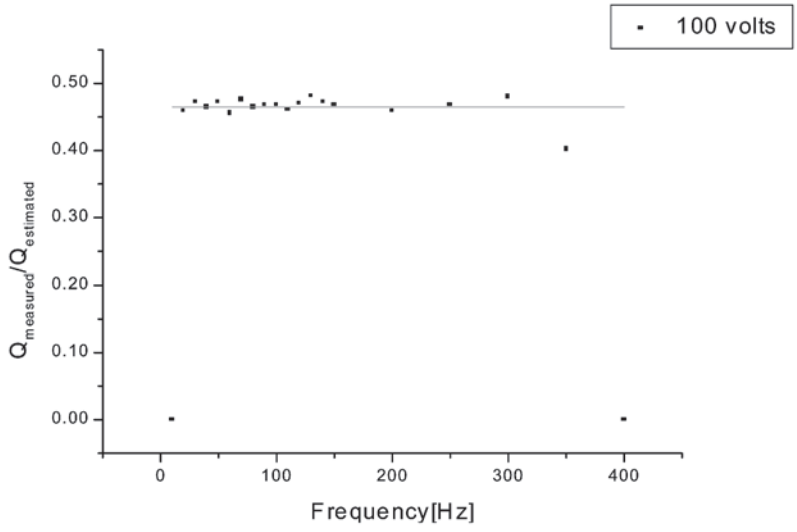

(b)

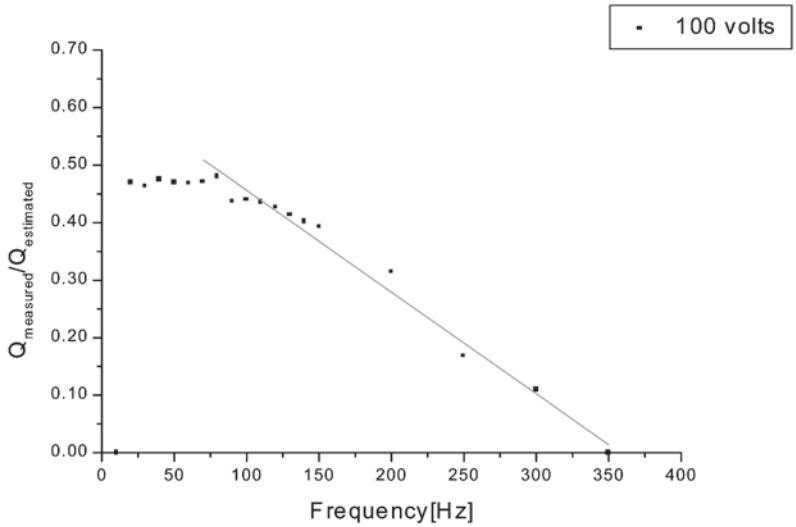

Fig. 10. Measured net flow rate, normalized by the estimated value: (a) microdiffuser prototype D100, (b) microdiffuser prototype D300.

cutoff frequency of 90 Hz and the estimated value of 57 Hz is mainly due to the error in the theoretical boundary layer thickness, estimated from the one-dimensional Stokes' flow model neglecting the three-dimensional geometry effect. From the unidirectional flow analysis of D300, the valve efficiency, (β_1–β_2) in eq. (3), is estimated as the frequency-independent value of 4.01×10^{-10}. On the other hand, the valve efficiency, (β_1

$-\beta_2$), estimated from the experimental results shown in Fig. 9(b) is frequency dependent and is obtained as 1.88×10^{-10} at 50 Hz and 6.73×10^{-11} at 250 Hz.

We also expect that the net flow rate in the D100 microdiffuser starts to decrease at the bidirectional flow frequencies greater than 500 Hz, at which the total boundary layer thickness is equal to the neck width of the microdiffuser. The constant ratio of the experimental flow rates to the theoretical values in Fig. 10 supports the validity of our dynamic flow model. Consequently, it is concluded that, as we expected in our dynamic flow model, the flow rectification performance and net flow capability of the microdiffuser valves tend to reduce when the total boundary layer thickness is smaller than the neck width of the microdiffuser.

6. Conclusions

We characterized the bidirectionally oscillating dynamic flow in planar microdiffusers and evaluated the frequency dependence of the flow rectification performance of the microdiffusers. In the theoretical study, we presented a theoretical model for the bidirectionally oscillating flow in planar microdiffusers, where the neck width and the boundary layer thickness govern the rectification performance of the microdiffuser. In the experimental study, we found that at low-frequency pumping, the net flow rates measured from the microdiffusers are approximately 47% of the values estimated from the unidirectional flow model. We also found that at high-frequency pumping, the net flow rates and the rectification performance of the microdiffusers are rapidly decreased when the total boundary layer thickness is smaller than the neck width. It is concluded that for a high flow rate or high rectification performance, the neck width of the microdiffuser should be smaller than the total boundary layer thickness developed at the maximum pump frequency.

References

1 M. A. Huff, M. S. Mettner, T. A. Lober and M. A. Schemidt: Proc. Solid-State Sensor and Actuator Workshop (South Carolina, 1990) p. 123.
2 H. Jerman: Proc. IEEE Solid-State Sensor and Actuator Workshop (South Carolina, 1990) p. 65.
3 K. Yanagisawa, H. Kuwano and A. Tago: Proc. Int. Conf. on Solid-State Sensors and Actuators (Transducers '93) (Yokohama, 1993) p. 102.
4 J. Behrens, A. Meckes and W. Benecke: Proc. Micro System Technologies (Potsdam, 1996) p. 820.
5 A. Meckes, J. Behrens and W. Benecke: Proc. Actuators 1998 (Bremen, 1998) p. 152.
6 E. Stemme and G. Stemme: Sensors and Actuatosr A **39** (1993) 159.
7 T. Gerlach: Sensors and Actuators A **69** (1998) 181.
8 A. Olsson, G. Stemme and E. Stemme: Proc. Micro Electro Mechanical Systems Workshop (San Diego, 1996) p. 378.
9 A. Olsson, G. Stemme and E. Stemme: Proc. Micro Electro Mechanical Systems Workshop (San Diego, 1996) p. 479.

10 A. Ullmann: Sensors and Actuators A **69** (1998) 97.
11 W. van der Wijngaart, H. Andersson, P. Enoksson, K. Noren and G. Stemme: Proc. Micro Electro Mechanical Systems Workshop (Miyazaki, 2000) p. 674.
12 S. Shoji: Topics in Current Chemistry **194** (1998) 163.
13 T. S. J. Lammerink, M. Elwenspoek and J. H. J. Fluitman: Proc. Micro Electro Mechanical Systems Workshop (Fort Lauderdale, 1993) p. 245.
14 G. Currie: Fundamental Mechanics of Fluids (McGraw-Hill, 1993) p. 228.